HHS Public Access

Author manuscript

Hepatology. Author manuscript; available in PMC 2018 January 01.

Published in final edited form as:

Hepatology. 2017 January ; 65(1): 32–43. doi:10.1002/hep.28873.

Expression of scavenger receptor-AI promotes alternative activation of murine macrophages to limit hepatic inflammation and fibrosis

Adam C. Labonte[*,†], **Sun-Sang J. Sung**[*,‡], **Lucas T. Jennelle**[*,†], **Aditya P. Dandekar**[*], and **Young S. Hahn**[*,†]

[*]Beirne B. Carter Center for Immunology Research, University of Virginia, Charlottesville, VA 22908

[†]Department of Microbiology, University of Virginia, Charlottesville, VA 22908

[‡]Department of Medicine & Center for Inflammation and Regeneration, University of Virginia, Charlottesville, VA 22908

Abstract

The liver maintains an immunologically tolerant environment as a result of continuous exposure to food and bacterial constituents from the digestive tract. Hepatotropic pathogens can take advantage of this niche and establish lifelong chronic infections causing hepatic fibrosis and hepatocellular carcinoma. Macrophages (Mϕ) play a critical role in regulation of immune responses to hepatic infection and regeneration of tissue. However, the factors crucial for Mϕ in limiting hepatic inflammation or resolving liver damage have not been fully understood. In this report, we demonstrate that the expression of C-type lectin receptor scavenger receptor-AI (SR-AI) is crucial for promoting M2-like Mϕ activation and polarization during hepatic inflammation. Liver Mϕ uniquely upregulated SR-AI during hepatotropic viral infection and displayed increased expression of alternative Mϕ activation markers such as YM-1, arginase-1, and IL-10 via the activation of Mertk associated with inhibition of mTOR. The expression of these molecules was reduced on Mϕ obtained from the livers of infected mice deficient for the gene encoding SR-AI (*msr1*). Furthermore, *in vitro* studies using an SR-AI-deficient Mϕ cell line revealed impeded M2 polarization and decreased phagocytic capacity. Direct stimulation with virus was sufficient to activate M2 gene expression in the wild type (WT) cell line but not in the knockdown cell line. Importantly, tissue damage and fibrosis were exacerbated in SR-AI$^{-/-}$ mice following hepatic infection and adoptive transfer of WT bone marrow derived Mϕ conferred protection against fibrosis in these mice. *Conclusion*: SR-AI expression on liver Mϕ promotes recovery from infection-induced tissue damage by mediating a switch to a pro-resolving Mϕ polarization state.

Corresponding author: Young S. Hahn, PhD, Carter Immunology Center, University of Virginia School of Medicine, P.O. Box 801386, Charlottesville, VA, USA 22908, Phone: 434-924-1155, Fax: 434-924-1221, ysh5e@virginia.edu.

The authors declare no conflict of interest.

Author contributions: AL, SS, and AD contributed to data acquisition and analysis. AL, LJ, AD, and YH contributed to study design and data interpretation. AL, SS, LJ, AD, and YH contributed to the writing and review of this report.

Keywords

SR-AI; M1; M2; polarization; fibrosis

Introduction

Due to constant exposure to typically inflammatory stimuli from the gut via the portal vein (i.e. debris from commensal bacteria), the liver has evolved out of necessity to maintain a tolerogenic environment (1). Subsequently, pathogens such as HCV have come to fill this niche and can establish lifelong chronic infections (2,3). While the liver is known to have remarkable regenerative capability, such persistent infections are characterized by liver fibrosis and cirrhosis, potentially leading to the development of hepatocellular carcinoma (4). The phenomenon of liver tolerance has been variously ascribed to dysfunctional activation of several immune cell compartments, including Mϕ (5). The specific role of Mϕ activation and the factors that control Mϕ activation, however, have not yet been well defined. In addition to monocytes and Mϕ circulating throughout the bloodstream, the liver contains a specialized tissue-resident Mϕ, the Kupffer cell, which is physically integrated into the structure of the sinusoid (6). Liver Mϕ are responsible for the maintenance of healthy tissue through phagocytic clearance of apoptotic cells and foreign materials and through tissue repair and remodeling during wound healing (7,8). Critically, Mϕ are also major regulators of the inflammatory response to disease and infection, monitoring the microenvironment through an array of surface receptors and secreting appropriate cytokines and chemokines (9).

Depending on the inflammatory insults they encounter, Mϕ populations can be directed to distinct phenotypic programs in a process known as Mϕ polarization (10). Classical activation is stimulated by microbial products and proinflammatory cytokines (IFNγ and/or LPS or TNF), and the resulting M1 Mϕ are characterized by high antigen presentation, high production of IL-12 and IL-23, and high production of nitric oxide (NO) and reactive oxygen intermediates (11). By contrast, alternative/M2 activation is mediated by IL-4, IL-10 and IL-13 and is characterized by little to no secretion of proinflammatory cytokines, increased secretion of anti-inflammatory cytokines, enhanced scavenging of cellular debris, and promotion of tissue remodeling and repair (12,13). M2 Mϕ also upregulate several endocytic surface receptors, including scavenger receptor A (SR-AI/CD204) (11,14).

Scavenger receptors are phagocytic pattern recognition receptors that mediate the clearance of both endogenous (modified host molecules, apoptotic cells) and exogenous (microbes, foreign particles) material (15). Scavenger receptor A exists in two isoforms (I and II) that are co-expressed mainly on Mϕ and have no functional differences; they are typically referred to collectively as SR-AI (16,17). Via its collagenous extracellular domain, SR-AI is capable of binding natural ligands (LTA and LPS) as well as non-physiological ligands (acetylated or oxidized low-density lipoprotein [LDL] and maleylated bovine serum antigen [BSA]) (16). Indeed, scavenger receptor expression and function have been linked to a number of diseases, including atherosclerosis, non-alcoholic steatohepatitis, hepatocellular carcinoma, and transplant rejection (10,18,19).

Many of these diseases may be linked to scavenger receptors via their involvement in Mϕ polarization: SR-AI acts as both a marker and an activator of M2 activation (20). Notably, scavenger receptor function is also linked to HCV infection in that both SR-AI and SR-B1 can recognize and endocytose HCV proteins (21,22). The exact function of SR-AI$^+$ Mϕ in hepatic viral infection, however, remains unknown. In the present study, we investigate the role of SR-AI expression by Mϕ in controlling tissue inflammation and repair during hepatic viral infection. This report shows that SR-AI expression on liver Mϕ protects against infection-induced tissue damage and fibrosis, possibly via mTOR-mediated modulation of M2 Mϕ polarization. These results provide insight into new targets for the design of therapeutic agents for chronic liver diseases caused by hepatic viral infections such as HCV.

Methods and Materials

Mice

6-8 week old female C57BL/6 and SR-AI$^{-/-}$ (B6.Cg-*Msr1*^{tm1Csk}/J) mice were purchased from Taconic Farms (Hudson, NY) and Jackson Laboratories (Sacramento, CA) respectively. Mice were housed in a pathogen-free facility and routinely tested for mouse hepatitis virus and other pathogens. Animals were handled according to protocols approved by the University of Virginia Institutional Animal Care and Use Committee.

Viral infection

Replication-defective recombinant adenovirus type 5 expressing ovalbumin (rAd5-OVA) under the human CMV promoter and lacking E1 and E3 genes were purchased from the Iowa Gene Transfer Vector Core (Iowa City, IA). Mice were injected intravenously with 5×10^7 IU AdOVA.

Hepatic and splenic mononuclear cell isolation

Mononuclear cells were isolated for further experimentation as described previously (23). Briefly, livers were passed through a metal spleen screen and digested with 0.05% collagenase IV (Sigma-Aldrich, St. Louis, MO) and intrahepatic mononuclear cells were purified via Histodenz density gradient centrifugation (Sigma-Aldrich, St. Louis, MO). Spleens were passed through a mesh spleen screen and mononuclear cells were purified by Ficoll gradient.

Flow cytometry and Luminex assay

Antibodies against MHC-II, Thy 1.2, F4/80, CD11b (eBioscience, Sand Diego, CA), and SR-AI (R&D Systems, Minneapolis, MN) were used for surface staining. 1.5×10^6 cells were blocked with anti-CD16/CD32 (2.4G2; University of Virginia, Charlottesville, VA) and incubated with the appropriate antibodies for 30 minutes at 4°C in Iscove's Modified Dulbecco's Medium (IMDM) supplemented with 2% fetal bovine serum (FBS) and 0.1% NaN_3. The cells were then washed and fixed in Cytofix/Cytoperm (BD Biosciences) according to the manufacturer's instructions prior to flow cytometry analysis. All samples were run on a BD FACS Canto II (BD Immunocytometry Systems, San Jose, CA) and analyzed using FlowJo software 8.8.6 (Tree Star Inc., Ashland, OR). For Luminex analysis, mononuclear cells were stained as above but in the absence of NaN_3 and without fixation.

The cells were resuspended in Hank's Buffered Salt Solution (HBSS) containing 1% fetal calf serum (FCS) and 1mM EDTA and sorted into F4/80^{hi}CD11b^{lo} KC or F4/80^{lo}CD11b^{hi} Mϕ using a BD Influx Cell Sorter at the Flow Cytometry Core Facility (University of Virginia, Charlottesville, VA). Sorted cell populations were cultured overnight in IMDM supplemented with 100 U/mL Pen Strep, 10% Hyclone FBS, 2 mM L-glutamine, and 10 μM β-mercaptoethanol. The resulting supernatants were submitted to the Flow Cytometry Core Facility for analysis using the Luminex MAGPIX assay system (Luminex, Austin, TX).

Fluorescent Microscopy

Samples were prepared for fluorescent microscopy as described previously (24). In brief, mouse livers were fixed with periodate-lysine-paraformaldehyde (PLP) fixative and mounted in optimal cutting temperature (OCT) medium before being sectioned at 5 μm, blocked in 2.4G2 solution, and stained with antibodies from Biolegend, eBioscience, and R&D Systems. Images were obtained with a Zeiss LSM-700 confocal microscope (Carl Zeiss MicroImaging GmbH, Jena, Germany).

Cell Culture

RAW 264.7 cells were obtained from ATCC and cultured in Dulbecco's Modified Eagle Medium (DMEM) supplemented with 10% FBS and 100 U/mL Pen Strep at 37°C and 5% CO_2. RAW cells were polarized by culturing 300,000 cells/well overnight in 24-well plates before replacing the medium with complete culture medium supplemented with either LPS (300 ng/mL), IL-4/IL-13 (20 ng/mL, 10 ng/mL), or dexamethasone (100 nM) and incubating for 2 hours at 37°C. For select experiments, RAW cells were cocultured overnight with AdOva in complete culture medium at an MOI of 0.5 or 5.0 PFU AdOVA.

Generation of msr1 Knockdown Cell Line

A panel of four 29-mer shRNA plasmids targeted against the murine *msr1* gene was generated by and obtained from OriGene (Rockville, MD). Each of the four anti-*msr*1 shRNA plasmids and the scramble control plasmid were packaged into lentiviral particles and transduced into RAW 264.7 cells following the manufacturer's instructions. The packaging plasmids ENV pCMV-VSVG, pRSV-REV, and Gag/Pol pMDLg/pRRE were kindly provided by Dr. Tim Bender (University of Virginia, Charlottesville, VA), amplified using OneShot TOP10 chemically competent *E. coli* (Invitrogen, Carlsbad, CA), and isolated using an Endotoxin-Free Plasmid Maxi Kit (Qiagen). Transduced RAW cells were isolated via puromycin selection and diluted to a single-cell suspension prior to subculturing.

Western blots

Cultured cells were lysed in buffer containing NaF, $Na_4P_2O_7$, Na_3VO_4, and protease inhibitor cocktail V (EMD Millipore, Temecula, CA) to preserve protein phosphorylation. Proteins were resolved on Mini-PROTEAN TGX precast gradient gels (BioRad, Berkeley, CA), transferred to PVDF membranes, and incubated with rabbit anti-phospho-mTOR (mAb, Cell Signaling Technology, Danvers, MA), anti-mTOR (mAb, Cell Signaling Technology), anti-phospho-MERTK (pAb, FabGennix, Frisco, TX), or anti-MERTK (pAb, FabGennix). The blots were then incubated with horseradish peroxidase (HRP)-linked anti-

rabbit IgG (pAb, Cell Signaling Technology) and HRP-linked goat anti-Actin (Santa Cruz Biotechnology, Santa Cruz, CA) and visualized with an 80/20 mix of SuperSignal West Pico Chemiluminescent Substrate and Femto Chemiluminescent Substrate (Thermo Scientific, Rochester, NY). Densitometry was performed using ImageJ analysis software (National Institute of Health, Bethesda, MD).

In vitro bead phagocytosis assay

RAW and MSRC2 cells were polarized as described above for 2 hours and washed with serum-free medium. A pre-warmed suspension of PE-conjugated FluoroSphere carboxylated beads (Molecular Probes, Eugene, OR) was added to the cells (500 μL serum-free medium and 1.5 μL beads per well) which were incubated for 2 hours at 37°C. The cells were washed 3 times with PBS and analyzed by flow cytometry. Quantification of internalized beads was determined by gating the PE histogram past the first peak to exclude beads stuck to the cell surface.

Adoptive transfer of BMDMs

Bone marrow was extracted from the femurs of WT C57BL/6 mice and cultured for 2 hours at 37°C in DMEM supplemented with 10% FBS, 100 U/mL Pen Strep, and 2 mM L-glutamine to adhere resident bone marrow Mϕ. The adherent cells were resuspended in culture medium containing 10% L-292 medium and allowed to differentiate for 7 days. The medium was replaced with fresh differentiation medium every 2 days. Recipient SR-AI$^{-/-}$ mice were treated with 100 μL clodronate liposome suspension (Encapsula NanoSciences, Brentwood, TN) via tail vein injection one day prior to transfer of 2×10^6 differentiated BMDMs, also via tail vein injection. Approximately 8 hours following BMDM transfer, the recipients were infected with 5×10^7 PFU AdOVA. The mice were sacrificed after 14 days for further experimentation.

Statistical analysis

Statistical significance was determined using either the two-tailed Student's *t* test or one-way analysis of variance (ANOVA) where appropriate. Analysis was performed using Prism software (GraphPad Software Inc., La Jolla, CA). Values of $p < 0.05$ were regarded as statistically significant. Asterisks (*, **, and ***) denote $p < 0.05$, $p < 0.01$, and $p < 0.001$, respectively.

Results

SR-AI is upregulated on Mϕ following hepatotropic viral infection

The expression of SR-AI has been reported to modulate the activation and polarization of Mϕ (20,25). To assess the impact of SR-AI expression on regulation of hepatic immune responses to infection and development of tissue damage, we injected 5e7 PFU of OVA-expressing adenovirus (AdOVA) into the tail vein of 6-8 week old C57BL/6 mice. The virus travels along the tail vein to the liver where the large majority is taken up by Mϕ and hepatocytes, establishing a hepatotropic infection. In order to fully examine the phenotype of SR-AI$^+$ liver Mϕ, we first determined the tempo and specificity of SR-AI expression in infection. Whole livers were harvested from AdOVA-infected mice and, following

homogenization and density gradient centrifugation, liver Mϕ were separately identified as liver-resident Kupffer cells (KC, F4/80^{hi}CD11b^{lo}) or non-resident circulating Mϕ (F4/80^{lo}CD11b^{hi}) by flow cytometry (Fig. 1A). Increased expression of SR-AI was observed on both KC and non-resident liver Mϕ seven days after AdOVA infection, a time point coinciding with viral clearance and the beginning of tissue repair (Fig. 1B, C). In contrast, there was no upregulation of SR-AI on splenic Mϕ following infection (Fig. 1B, C), suggesting that the specific upregulation of SR-AI on liver Mϕ was possibly a result of viral recognition at the site of infection. Importantly, fluorescent microscopy of histochemically stained liver sections confirmed upregulation of SR-AI detected by flow cytometry and also revealed that SR-AI^{+} liver Mϕ co-expressed the M2 surface marker YM-1 (Fig. 1D). Taken together, these results suggest that SR-AI may trigger signaling involved in alternative activation in liver Mϕ during hepatotropic viral infection.

SR-AI modulates Mϕ activation upon viral insult

We next investigated whether the increase in SR-AI expression following infection indeed correlated with a shift in Mϕ activation. Luminex analysis of FACS-sorted KC and circulating Mϕ showed that production of the M2 cytokine IL-10 by both populations was increased on day 7 post-infection (Fig. 2A). KC tended to produce higher levels of IL-10 compared to non-resident Mϕ Several proinflammatory mediators typical of M1 activation (IL-6, MIP-1α, and MIP-1β) were also secreted by these cells in both naive and infected conditions, suggesting that liver Mϕ may assume an “M2-like” intermediate phenotype with some M1 characteristics (Fig. 2A).

Based on the finding that SR-AI^{+} Mϕ in the liver exhibited M2-like characteristics, we examined the status of Mϕ activation in WT and SR-AI$^{-/-}$ animals to determine whether SR-AI expression contributes to M2 polarization. Indeed, when Mϕ-enriched mononuclear liver cell fractions from infected animals were analyzed by qPCR, liver Mϕ in SR-AI$^{-/-}$ mice were impaired in their expression of the M2 genes *arg1*, *chi313* (YM-1), and *il-10* (Fig. 2B). Interestingly, expression of the M1 gene *nos2* was also reduced in the cells obtained from SR-AI$^{-/-}$ mice compared to WT controls. When sorted SR-AI$^{-/-}$ Mϕ and KC were analyzed by Luminex, both populations upregulated IL-10 secretion following infection but to a lesser degree than their WT counterparts (Fig. 2C). We next asked whether SR-AI$^{-/-}$ Mϕ had lost the ability to become alternatively activated by attempting to force M2 polarization via 2-hour stimulation with IL-4 and IL-13. Both the WT and SR-AI$^{-/-}$ Mϕ were capable of upregulating *arg1* expression in the presence of these strong M2 stimuli, but the level of Arg-1 expression by SR-AI$^{-/-}$ cells was still lower than WT cells (Fig. 2D).

Mice deficient in SR-AI develop exacerbated infection-induced liver tissue damage and fibrosis

Given the timing of the appearance of SR-AI^{+} Mϕ in the course of infection and their potential role in wound repair and tissue remodeling following injury and infection, we performed histological examinations on liver sections from WT and SR-AI$^{-/-}$ mice to interrogate possible protective qualities of SR-AI expression. Post-infection liver tissue damage appeared dramatically more severe in the absence of SR-AI. H&E staining of liver tissue sections showed increased inflammatory infiltrates in the SR-AI$^{-/-}$ mice compared to

WT at 7 and 14 days post-infection (Fig. 3A). Infection-induced hepatocyte DNA damage was also increased in the absence of SR-AI as measured by TUNEL staining (Fig. 3B). Collagen staining by Trichrome C revealed deposition of extracellular matrix between cells (in blue) in the knockout liver 14 dpi (Fig. 3C). No positive staining was observed in the WT liver at day 14 or in either mouse at day 7 post-infection. Together, these data suggest that the expression of SR-AI on liver Mϕ plays a protective role in viral infection. SR-AI^{+} liver Mϕ may thus comprise an alternatively activated subset involved in wound repair and tissue remodeling.

SR-AI expression is required for modulation of Mϕ activation via mTOR and maintaining phagocytic ability

In order to further investigate a direct effect of SR-AI on Mϕ activation and function, we established a cell line that recapitulated the SR-AI$^{-/-}$ mice. To accomplish this, plasmids containing shRNA sequences targeted against the *msr1* gene were loaded into lentivirus particles via a lentiviral packaging cell line. These lentiviruses were then administered to the RAW 264.7 murine Mϕ cell line, after which individually infected cells were clonally expanded and tested for knockdown efficiency via flow cytometry of SR-AI and qPCR of *msr1*. Subclones MSRC1 and MSRC2 showed significant knockdown of *msr1* message, but MSRC2 showed more dramatic reduction in SR-AI surface expression than that in MSRC1 (Fig. 4A, B). Stable SR-AI knockdown persisted through at least 20 passages in culture, as well as through freeze-thaw cycles (data not shown). The RAW 264.7 cell line (hereafter referred to as RAW cells) can be reliably polarized *in vitro* via stimulation with LPS (M1) or IL-4/IL-13 (M2). We confirmed Mϕ polarization using real-time PCR for the prototypical M1 and M2 genes arginase (*arg1*) and iNos (*nos2*) (Supporting Fig. S1A). Notably, *msr1* gene expression appeared to track with M2 polarization (Supporting Fig. S1B). When exposed to M2 stimuli, RAW cells exhibit robust upregulation of *arg1* and *chi313* (encoding YM1) while MSRC2 cells show minimal upregulation, in agreement with the results obtained from SR-AI$^{-/-}$ mice (Fig. 4C). The lipid metabolism gene *srebf1* was included as an irrelevant control, and remained unchanged in the knockdown cell line under all stimulation conditions (Fig. 4D).

While stimulation with LPS or IL-4/IL-13 are reliable ways to induce specific aspects of Mϕ polarization, we speculated that viral infection represented a unique mode of stimulation via SR-AI-mediated recognition, and therefore we attempted to stimulate RAW and MSRC2 cells by directly adding AdOVA *in vitro*. Overnight incubation with virus was enough to stimulate upregulation of both *arg1* and *nos2* and the *nos2* effect was dose-dependent with viral MOI (*arg1* expression actually decreased slightly at 0.5 MOI when compared to uninfected). Strikingly, *Arg1* expression by MSRC2 cells remained unchanged upon addition of virus, and *nos2* upregulation was only observed at 5.0 MOI and to a very small degree when compared to the RAW cell expression (Fig. 4E). Interestingly, RAW cells exhibited decreased phagocytosis with 0.5 MOI of virus compared to uninfected cells but this deficit was absent with 5.0 MOI of virus. However, at a higher dose of virus, bead uptake by MSRC2 cells progressively decreased and MSRC2 cells treated with 5.0 MOI of virus were able to internalize fewer beads than their RAW counterparts (Fig. S2A, B).

We next sought to investigate the mechanism by which SR-AI expression alters Mϕ gene expression. While many studies implicate SR-AI signaling in biological processes, the exact mechanism remains unclear. Previous reports that activation of mammalian target of rapamycin (mTOR) regulates scavenger receptor expression lead us to investigate whether mTOR phosphorylation could in turn be regulated by expression of SR-AI (26,27). When analyzed by Western blot, SR-AI knockdown cells exhibited enhanced mTOR phosphorylation compared to SR-AI sufficient cells under all stimulation conditions (Fig. 4F, S3A). While SR-AI possesses no recognized intracellular signaling motif, it has been suggested that SR-AI associates with Mer receptor tyrosine kinase (Mertk) in order to transduce signals (28). Indeed, Western blot analysis revealed Mertk phosphorylation to be impaired in SR-AI knockdown cells stimulated with M1 or M2 cocktails as compared to their WT counterparts (Fig. 4F, S3B). Taken together, these results suggest that the activation of Mertk may lead to inhibition of the mTOR pathway and be involved in SR-AI-mediated alteration of Mϕ activation.

Transfer of SR-AI$^+$ Mϕ into SR-AI-deficient mice protects against infection-induced tissue damage and fibrosis

We next investigated whether SR-AI$^+$ Mϕ are able to protect from the development of fibrosis in SR-AI$^{-/-}$ mice. First, SR-AI$^{-/-}$ mice were treated with clodronate to deplete the endogenous liver Mϕ population before receiving an adoptive transfer of WT BMDMs intravenously (Fig. 5A). Transfer of SR-AI$^+$ Mϕ derived from WT mice was verified by the presence of SR-AI$^+$ Mϕ in SR-AI$^{-/-}$ recipient mice (Fig. 5C). The animals were then infected with AdOVA for 14 days and the degree of liver fibrosis was assessed by Trichrome C staining. Remarkably, while the SR-AI$^{-/-}$ mice accumulate a significant degree of fibrosis, knockout mice that received WT BMDMs prior to infection did not develop fibrosis similar to that of WT mice (Fig. 5B). These results suggest that manipulation of SR-AI signaling and adoptive transfer of SR-AI$^+$ Mϕ may represent potential therapeutic targets for preventing the development of hepatic fibrosis.

Discussion

The liver is a highly regenerative organ with a unique immune repertoire that houses over 80% of the body's macrophages, including liver-resident KC and non-circulating Mϕ These Mϕ play a unique role in maintaining homeostatic immune tolerance in the liver, and as described in this report, orchestrate inflammatory responses and restore tissue homeostasis following injury. Here, we describe the functional characteristics of SR-AI$^+$ Mϕ and their protective role in fibrosis development during hepatotropic viral infection. SR-AI expression steadily increases at later time points in infection, which parallels the ability of SR-AI$^+$ Mϕ to produce anti-inflammatory mediators, express M2-like markers, perform efficient phagocytosis, and limit the deposition of fibrotic tissue. Collectively, these observations identify SR-AI as a key regulator and potential target in preventing liver fibrosis.

As a scavenger receptor, SR-AI can bind a variety of polyanionic ligands, including LDL, bacterial products, polysaccharides, and nucleic acids. Interestingly, M2-like features were reduced in SR-AI$^{-/-}$ mice (both *in vivo* and under M2-polarizing conditions *ex vivo*) and *in*

vitro in cultured Mϕ with deficient SR-AI expression. Given that each of these conditions is likely to have a different composition of SR-AI ligands, the similarities in Mϕ phenotypes indicate that the identity of the ligands might not be crucial for determining the polarizing function of SR-AI. Rather, SR-AI signaling upon engagement with specific ligands may play a pivotal role in influencing M2-like Mϕ polarization. However, expression of iNOS (typically associated with M1 polarization) was decreased in Mϕ from the SR-AI$^{-/-}$ animals, tracking with the M2-like phenotype exhibited by SR-AI^{+} Mϕ. Differences in the quality and quantity of SR-AI ligands may underlie this mosaic polarization phenotype. Furthermore, redundancy in scavenger receptor repertoires and other polarizing factors may be driving these intermediate polarization states. Indeed, the loss of M2-like features was more pronounced in cell lines lacking expression of SR-AI when compared to SR-AI$^{-/-}$ mice, underscoring that Mϕ polarization *in vivo* includes a spectrum of activation states rather than absolute M1 or M2 phenotypes. Recent reports have also shown that production of pro-inflammatory mediators by M2 Mϕ subsets is not uncommon (31–33). It is therefore likely that the polarization state of SR-AI^{+} liver Mϕ following viral infection represents a crossover M2-like state with some M1 features. SR-AI modulates this entire phenotype, so when arginase induction is inhibited in SR-AI-deficient animals and cell lines, iNOS expression tracks with this phenotype. Moreover, the inhibition of M2 polarization in SR-AI deficient Mϕ RAW cells occurred in the complete absence of potential physiological stimuli such as apoptotic cells or viral particles. This finding indicates that in addition to its role during infection, SR-AI contributes to the M2 polarization signaling pathway even under homeostatic conditions.

Intriguingly, SR-AI was differentially expressed in liver Mϕ and KC: SR-AI expression peaked in liver Mϕ at day 7 post-infection and returned to basal levels by day 14. In contrast, KC expression of SR-AI was maintained at high levels from day 7 to day 21 post-infection. These differences prompt interesting questions regarding distinct functions of these two Mϕ populations. A likely explanation of these differences is that KC are the predominant M2-like cells mediating tissue recovery in hepatotropic viral infection as they continue to express high levels of the M2-promoting marker SR-AI. KC are thought to arise from liver-resident yolk-sac derived precursors; meanwhile, non-resident liver Mϕ are derived from monocyte precursors from the bone marrow. Although there is limited information regarding the expression of SR-AI during Mϕ development, it is possible that expression of SR-AI and other M2 effectors are programmed into liver-resident Mϕ precursors. However, deposition of fibrotic tissue was minimized upon transfer of SR-AI^{+} BMDMs into SR-AI$^{-/-}$ mice, suggesting that the local tolerogenic environment may also induce SR-AI and other M2-like properties in Mϕ originating from extrahepatic sources. Furthermore, the balance of M1 and M2 Mϕ at the site of infection is directly related to the development and progression of tissue injury. While pro-resolving M2 Mϕ subsets are responsible for the resolution of inflammation and the clearance and remodeling of scar tissue, M1 Mϕ (or even other M2 Mϕ subsets) can actively contribute to production of extracellular matrix and further tissue damage. Our studies report that SR-AI^{+} liver Mϕ are necessary for optimal recovery from infection, as measured by the presence of inflammatory infiltrates, fibrotic lesions, and hepatocellular DNA damage (Fig. 3A-C).

The molecular and cellular cues that program Mϕ activation thus require further investigation and may have significant implications for the development and function of these cells. Our findings implicate SR-AI expression as a possible driver of alternative Mϕ activation in hepatotropic viral infection. The balance between M1 and M2 Mϕ activation (and additional subtypes of M2 Mϕ) is a key determinant of recovery from tissue injury and progression to fibrosis. Consequently, the idea that the scavenger receptor SR-AI acts as a switch to turn on resolution of inflammation and repair of tissue injury is a promising avenue to understand Mϕ polarization in the pathogenesis of chronic liver diseases.

Supplementary Material

Refer to Web version on PubMed Central for supplementary material.

Acknowledgments

Financial support statement: This work was supported by National Institute of Health Grants R01DK063222 and U19AI083024.

Abbreviations

HCV	hepatitis C Virus
Mϕ	macrophage
SR-AI	scavenger receptor AI
WT	wild type
AdOVA	adenovirus expressing ovalbumin
mTOR	mammalian target of rapamycin
Mertk	mer receptor tyrosine kinase
BMDM	bone marrow derived macrophage

References

1. Knolle PA, Gerken G. Local control of the immune response in the liver. Immunol. Rev. 2000; 174:21–34. [PubMed: 10807504]
2. Dustin LB, Cashman SB, Laidlaw SM. Immune control and failure in HCV infection--tipping the balance. J. Leukoc. Biol. 2014; 96:535–48. [PubMed: 25015956]
3. Hoofnagle JH. Course and outcome of hepatitis C. Hepatology. 2002; 36:S21–9. [PubMed: 12407573]
4. Manickam C, Reeves RK. Modeling HCV disease in animals: virology, immunology and pathogenesis of HCV and GBV-B infections. Front. Microbiol. 2014; 5:690. [PubMed: 25538700]
5. Crispe IN. Immune tolerance in liver disease. Hepatology. 2014; 60:2109–17. [PubMed: 24913836]
6. Strauss O, Dunbar PR, Bartlett A, Phillips A. The immunophenotype of antigen presenting cells of the mononuclear phagocyte system in normal human liver--a systematic review. J. Hepatol. 2015; 62:458–68. [PubMed: 25315649]
7. Chen Q, Xue Y, Sun J. Kupffer cell-mediated hepatic injury induced by silica nanoparticles in vitro and in vivo. Int. J. Nanomedicine. 2013; 8:1129–40. [PubMed: 23515466]

8. You Q, Holt M, Yin H, Li G, Hu C-J, Ju C. Role of hepatic resident and infiltrating macrophages in liver repair after acute injury. Biochem. Pharmacol. 2013; 86:836–43. [PubMed: 23876342]
9. Boltjes A, Movita D, Boonstra A, Woltman AM. The role of Kupffer cells in hepatitis B and hepatitis C virus infections. J. Hepatol. 2014; 61:660–71. [PubMed: 24798624]
10. Labonte AC, Tosello-Trampont A-C, Hahn YS. The role of macrophage polarization in infectious and inflammatory diseases. Mol. Cells. 2014; 37:275–85. [PubMed: 24625576]
11. Mantovani A, Sica A, Sozzani S, Allavena P, Vecchi A, Locati M. The chemokine system in diverse forms of macrophage activation and polarization. Trends Immunol. 2004; 25:677–86. [PubMed: 15530839]
12. Martinez FO, Helming L, Gordon S. Alternative activation of macrophages: an immunologic functional perspective. Annu. Rev. Immunol. 2009; 27:451–83. [PubMed: 19105661]
13. Alfano M, Graziano F, Genovese L, Poli G. Macrophage Polarization at the Crossroad Between HIV-1 Infection and Cancer Development. Arterioscler. Thromb. Vasc. Biol. 2013; 33:1145–52. [PubMed: 23677880]
14. Gordon S. Alternative activation of macrophages. Nat. Rev. Immunol. 2003; 3:23–35. [PubMed: 12511873]
15. Penberthy KK, Ravichandran KS. Apoptotic cell recognition receptors and scavenger receptors. Immunol. Rev. 2016; 269:44–59. [PubMed: 26683144]
16. Bowdish DME, Gordon S. Conserved domains of the class A scavenger receptors: evolution and function. Immunol. Rev. 2009; 227:19–31. [PubMed: 19120472]
17. Martínez VG, Moestrup SK, Holmskov U, Mollenhauer J, Lozano F. The Conserved Scavenger Receptor Cysteine-Rich Superfamily in Therapy and Diagnosis. 2011; 63:967–1000.
18. Yu X, Guo C, Fisher PB, Subjeck JR, Wang X-Y. Scavenger Receptors: Emerging Roles in Cancer Biology and Immunology. Adv. Cancer Res. 2015; 128:309–64. [PubMed: 26216637]
19. Kzhyshkowska J, Neyen C, Gordon S. Role of macrophage scavenger receptors in atherosclerosis. Immunobiology. 2012; 217:492–502. [PubMed: 22437077]
20. Hu Y, Zhang H, Lu Y, Bai H, Xu Y, Zhu X. Class A scavenger receptor attenuates myocardial infarction-induced cardiomyocyte necrosis through suppressing M1 macrophage subset polarization. Basic Res. Cardiol. 2011:1311–1328. [PubMed: 21769674]
21. Beauvillain C, Meloni F, Sirard J-C, Blanchard S, Jarry U, Scotet M, et al. The scavenger receptors SRA-1 and SREC-I cooperate with TLR2 in the recognition of the hepatitis C virus non-structural protein. 3 by dendritic cells. J. Hepatol. 2010; 52:644–51. [PubMed: 20338659]
22. Syder AJ, Lee H, Zeisel MB, Grove J, Soulier E, Macdonald J, et al. Small molecule scavenger receptor BI antagonists are potent HCV entry inhibitors. J. Hepatol. 2011; 54:48–55. [PubMed: 20932595]
23. Dolina JS, Braciale TJ, Hahn YS. Liver-primed CD8+ T cells suppress antiviral adaptive immunity through galectin-9-independent T-cell immunoglobulin and mucin. 3 engagement of high-mobility group box. 1 in mice. Hepatology. 2014; 59:1351–65. [PubMed: 24677194]
24. Krueger PD, Kim TS, Sung S-SJ, Braciale TJ, Hahn YS. Liver-resident CD103+ dendritic cells prime antiviral CD8+ T cells in situ. J. Immunol. 2015; 194:3213–22. [PubMed: 25712214]
25. Zhu X, Zong G, Zhu L, Jiang Y, Ma K, Zhang H, et al. Deletion of class A scavenger receptor deteriorates obesity-induced insulin resistance in adipose tissue. Diabetes. 2014; 63:562–77. [PubMed: 24170693]
26. Fruhwürth S, Krieger S, Winter K, Rosner M, Mikula M, Weichhart T, et al. Inhibition of mTOR down-regulates scavenger receptor, class B, type I (SR-BI) expression, reduces endothelial cell migration and impairs nitric oxide production. Biochim. Biophys. Acta - Mol. Cell Biol. Lipids. 2014; 1841:944–953.
27. Mwaikambo BR, Yang C, Chemtob S, Hardy P. Hypoxia up-regulates CD36 expression and function via hypoxia-inducible factor-1- and phosphatidylinositol 3-kinase-dependent mechanisms. J. Biol. Chem. 2009; 284:26695–707. [PubMed: 19640849]
28. Todt JC, Hu B, Curtis JL. The scavenger receptor SR-A I/II (CD204) signals via the receptor tyrosine kinase Mertk during apoptotic cell uptake by murine macrophages. J. Leukoc. Biol. 2008; 84:510–518. [PubMed: 18511575]

29. Gensel JC, Zhang B. Macrophage activation and its role in repair and pathology after spinal cord injury. Brain Res. 2015; 1619:1–11. [PubMed: 25578260]

30. Keeler GD, Durdik JM, Stenken JA. Localized delivery of dexamethasone-21-phosphate via microdialysis implants in rat induces M(GC) macrophage polarization and alters CCL2 concentrations. Acta Biomater. 2015; 12:11–20. [PubMed: 25449921]

31. Ohtsuki T, Kimura K, Tokunaga Y, Tsukiyama-Kohara K, Tateno C, Hayashi Y, et al. M2 Macrophages Play Critical Roles in Progression of Inflammatory Liver Disease in Hepatitis C Virus Transgenic Mice. J. Virol. 2015; 90:300–7. [PubMed: 26468521]

32. Saha B, Kodys K, Szabo G. Hepatitis C Virus-Induced Monocyte Differentiation Into Polarized M2 Macrophages Promotes Stellate Cell Activation via TGF-β. C. Cell. Mol. Gastroenterol. Hepatol. 2016

33. Poczobutt JM, De S, Yadav VK, Nguyen TT, Li H, Sippel TR, et al. Expression Profiling of Macrophages Reveals Multiple Populations with Distinct Biological Roles in an Immunocompetent Orthotopic Model of Lung Cancer. J. Immunol. 2016; 196:2847–59. [PubMed: 26873985]

34. Dansako H, Yamane D, Welsch C, McGivern DR, Hu F, Kato N, et al. Class A scavenger receptor 1 (MSR1) restricts hepatitis C virus replication by mediating toll-like receptor. 3 recognition of viral RNAs produced in neighboring cells. PLoS Pathog. 2013:9.

35. DeWitte-Orr SJ, Collins SE, Bauer CMT, Bowdish DM, Mossman KL. An accessory to the “Trinity”: SR-As are essential pathogen sensors of extracellular dsRNA, mediating entry and leading to subsequent type I IFN responses. PLoS Pathog. 2010:6.

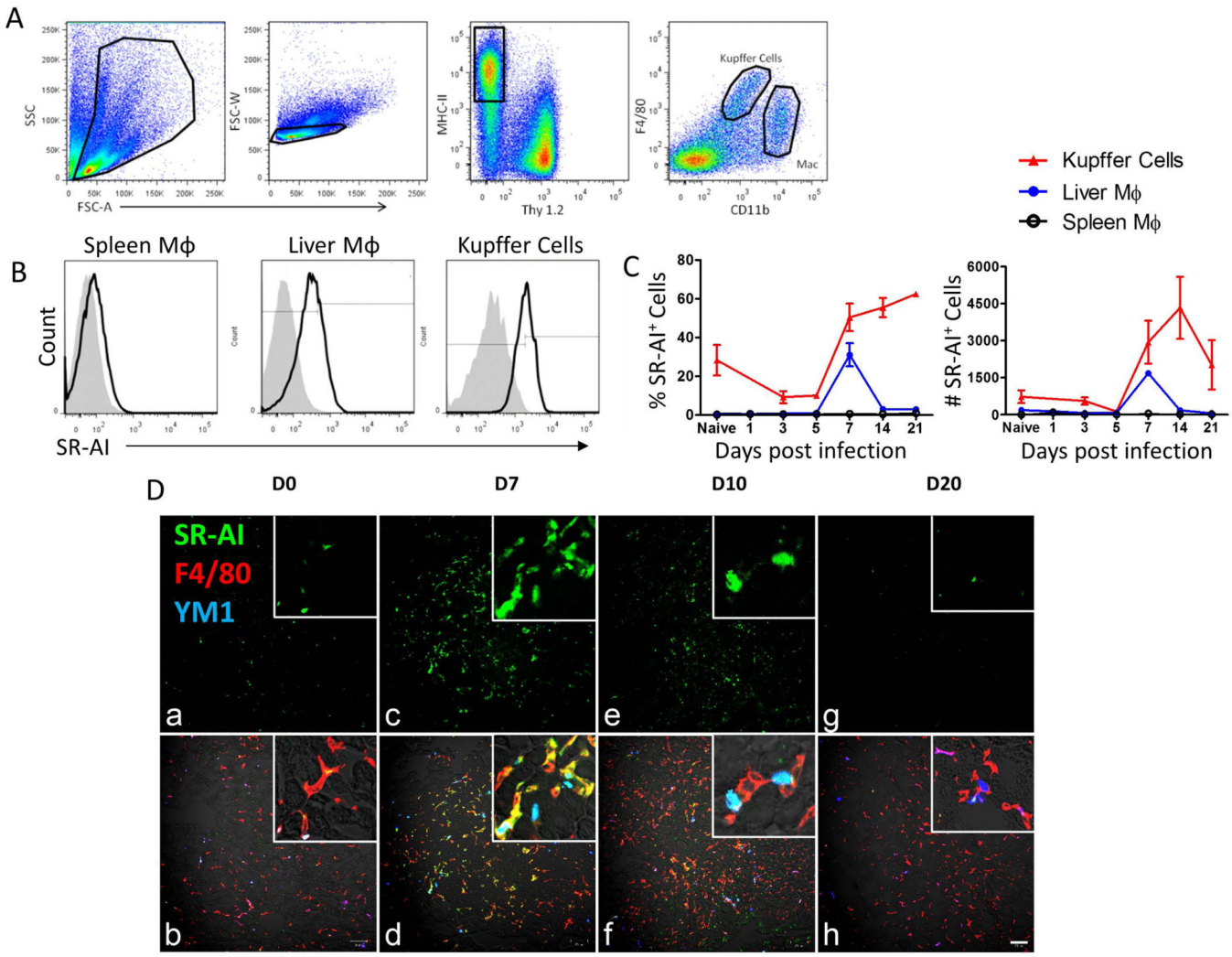

Figure 1. SR-AI is upregulated on Mϕ following hepatic viral infection

(**A**) Flow cytometry gating strategy for liver macrophages. Mononuclear cells were separated from whole liver homogenate via density gradient centrifugation and live singlets were gated on Thy1.2^{-}MHC-II^{+}. F4/80^{hi}CD11b^{mid} cells were identified as liver resident Kupffer cells and F4/80^{mid}CD11b^{hi} cells were identified as non-resident macrophages. (**B**) SR-AI surface expression (black trace) vs isotype control (gray histogram) in spleen Mϕ, liver Mϕ, and Kupffer cells at day 7 post infection. (**C**) Time course of frequency and number of SR-AI^{+} cells (determined by gating on isotype control) during AdOVA infection. Data points are mean±SEM of n=3 mice. (**D**) Immunofluorescence microscopy of sections from AdLacZ infected mouse liver at 0, 7, 10, and 20 days post infection (× 100 magnification and scale bar = 100 μm, insert × 200 magnification). Panels a, c, e, and g show SR-AI single surface staining in green; panels b, d, f, and h show merged staining of SR-AI (green), F4/80 (red), and YM1 (blue).

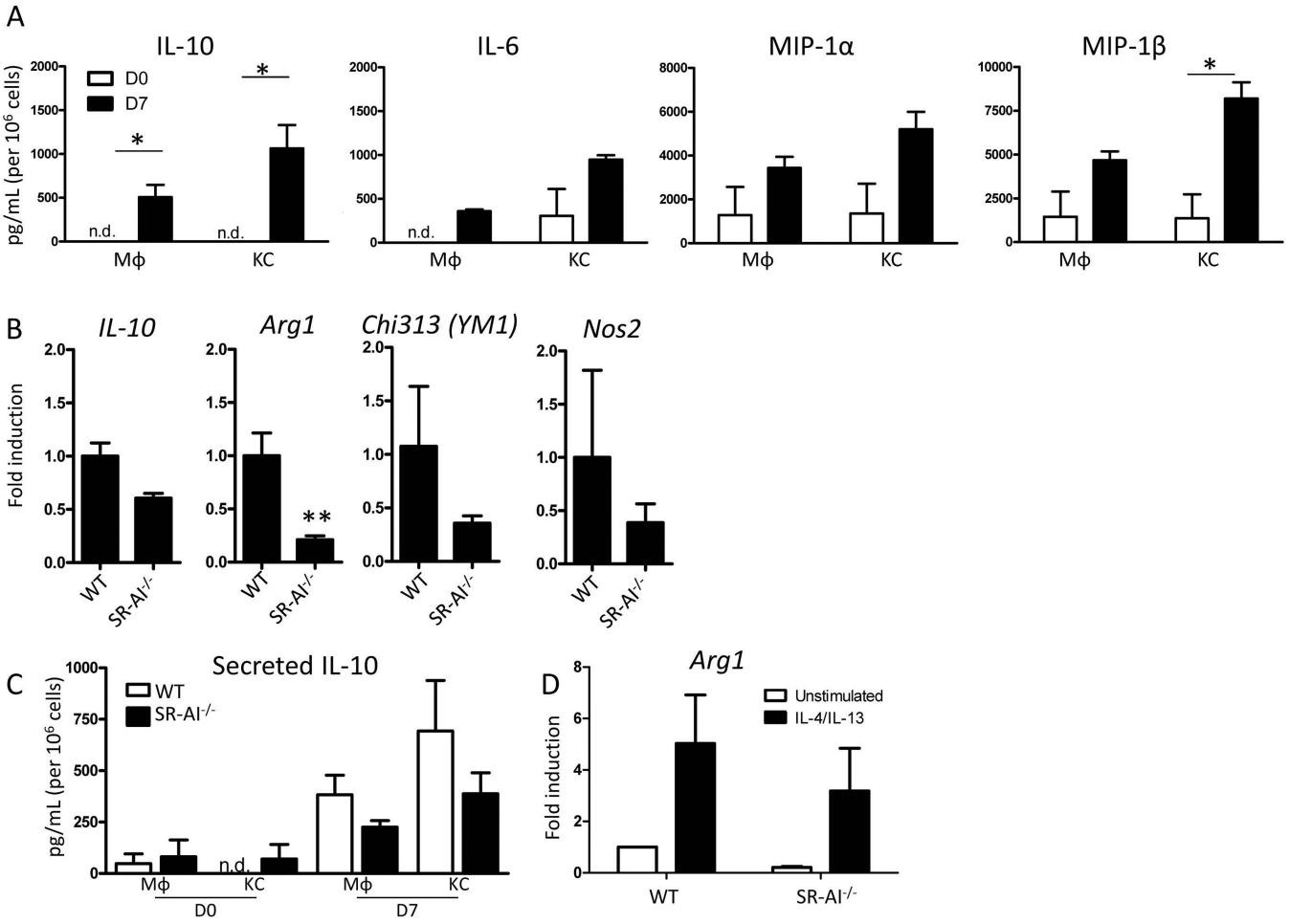

Figure 2. SR-AI modulates Mϕ activation upon viral insult

(**A**) Luminex quantification of cytokines and chemokines in supernatants collected from FACS sorted liver KCs and Mϕ from infected WT mice following overnight culture. Data are mean±SEM of n=3 mice. (**B**) qPCR analysis for expression of M2-related genes in Mϕ-enriched mononuclear cell fractions from WT and SR-AI$^{-/-}$ livers on day 7 post infection. Expression levels were calculated via the ddCT method and normalized to HPRT expression, data are mean±SEM for n=3 mice. (**C**) Luminex data of IL-10 levels in supernatants from sorted Mϕ or KC from WT and SR-AI$^{-/-}$ mice at day 7 post infection. Data are mean±SEM for n=3 mice. (**D**) Arginase 1 qPCR analysis of Mϕ from infected WT or SR-AI$^{-/-}$ livers cultured for 2h in either plain media or media with IL-4 and IL-13 to induce M2 polarization. Expression levels were calculated as in **A**, data are mean±SEM for n=3 mice.

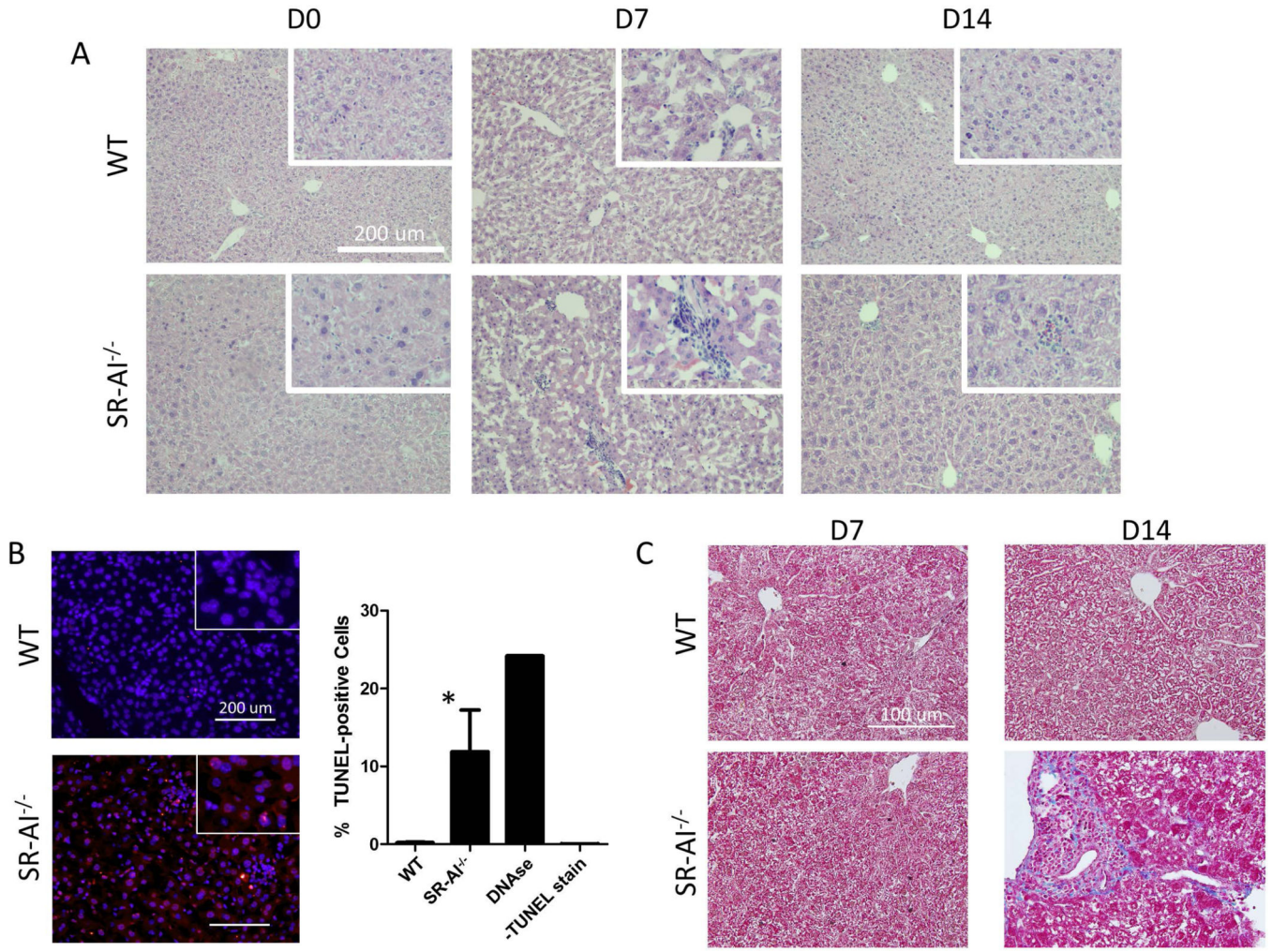

Figure 3. Infection-induced tissue damage is more severe in the absence of SR-AI

(**A**) H&E staining of liver sections obtained from WT and SR-AI$^{-/-}$ mice 0, 7, or 14 days after tail vein injection of 5e7 PFU of AdOVA (× 100 magnification and scale bars = 200 μm, insert × 200 magnification). Images are representative of 3 independent experiments. (**B**) Visualization of cell damage by TUNEL staining of WT and SR-AI$^{-/-}$ liver sections 7 days post infection (× 100 magnification and scale bars = 200 μm, insert × 200 magnification). Staining was quantified by dividing the number of positive red stained cells by the total number of blue counter stained cells. Data are mean±SEM, *P<0.05 vs WT mice. (**C**) Trichrome staining for collagen in liver sections from WT and SR-AI$^{-/-}$ mice 7 and 14 days post infection (×100 magnification and scale bars = 200 μm). Images are representative of 3 independent experiments.

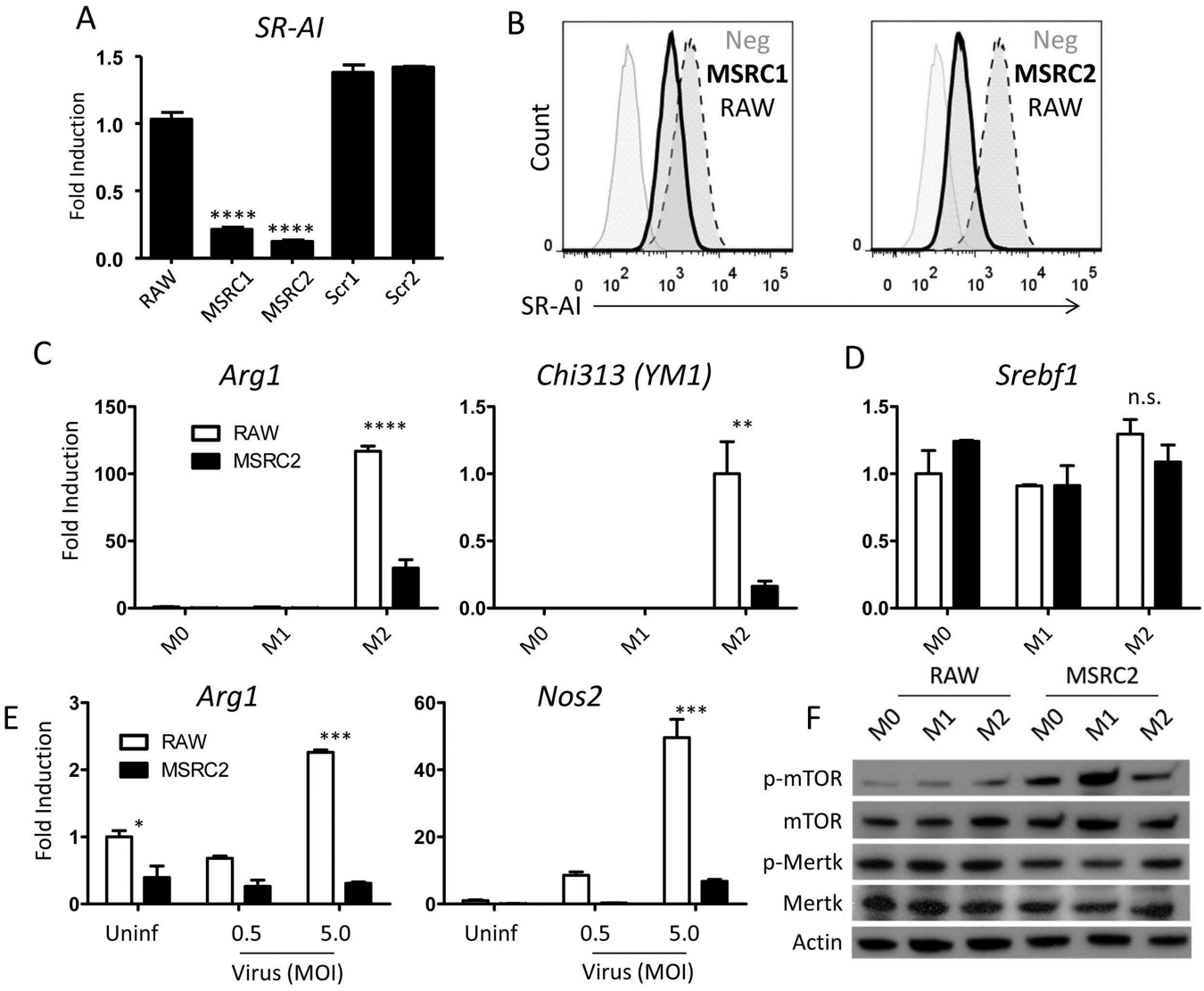

Figure 4. Generation of a stable MSR knockdown cell line

(**A**) qPCR analysis of relative *Msr1* expression in two subcultures of siRNA-transfected cells and two subcultures transfected with scrambled control plasmids. Expression levels were calculated via the ddCT method and normalized to HPRT expression, then normalized to expression of untransfected RAW cells. Data are mean±SEM for n=3, ****P<0.00005. (**B**) Flow analysis of SR-AI expression after transfection with lentivirally-packaged anti-*Msr1* siRNA. The bold trace represents transfected RAW cell subclones while the dotted trace represents WT RAW cells. (**C,D**) qPCR analysis comparing *arg1*, *chi313*, and *srebf1* expression by stable knockdown MSRC2 cells to that of untransfected RAW cells. Expression levels were calculated as in **A**. Data are mean±SEM for n=3; **P<0.005, ****P<0.00005. (**E**) *Arg1* and *Nos2* gene expression of MSRC2 and untransfected RAW cells following overnight coculture with 0, 0.5 MOI, or 5.0 MOI of AdOVA in complete media. Expression levels were calculated as in **A**, data are mean±SEM for n=3. (**F**) Western blot of phosphorylated and total mTOR and Mertk from whole cell lysates of RAW or

MSRC2 cells incubated for 2 hours in either plain media (M0), LPS (M1), or IL-4 and IL-13 (M2). Images are representative of 3 independent experiments.

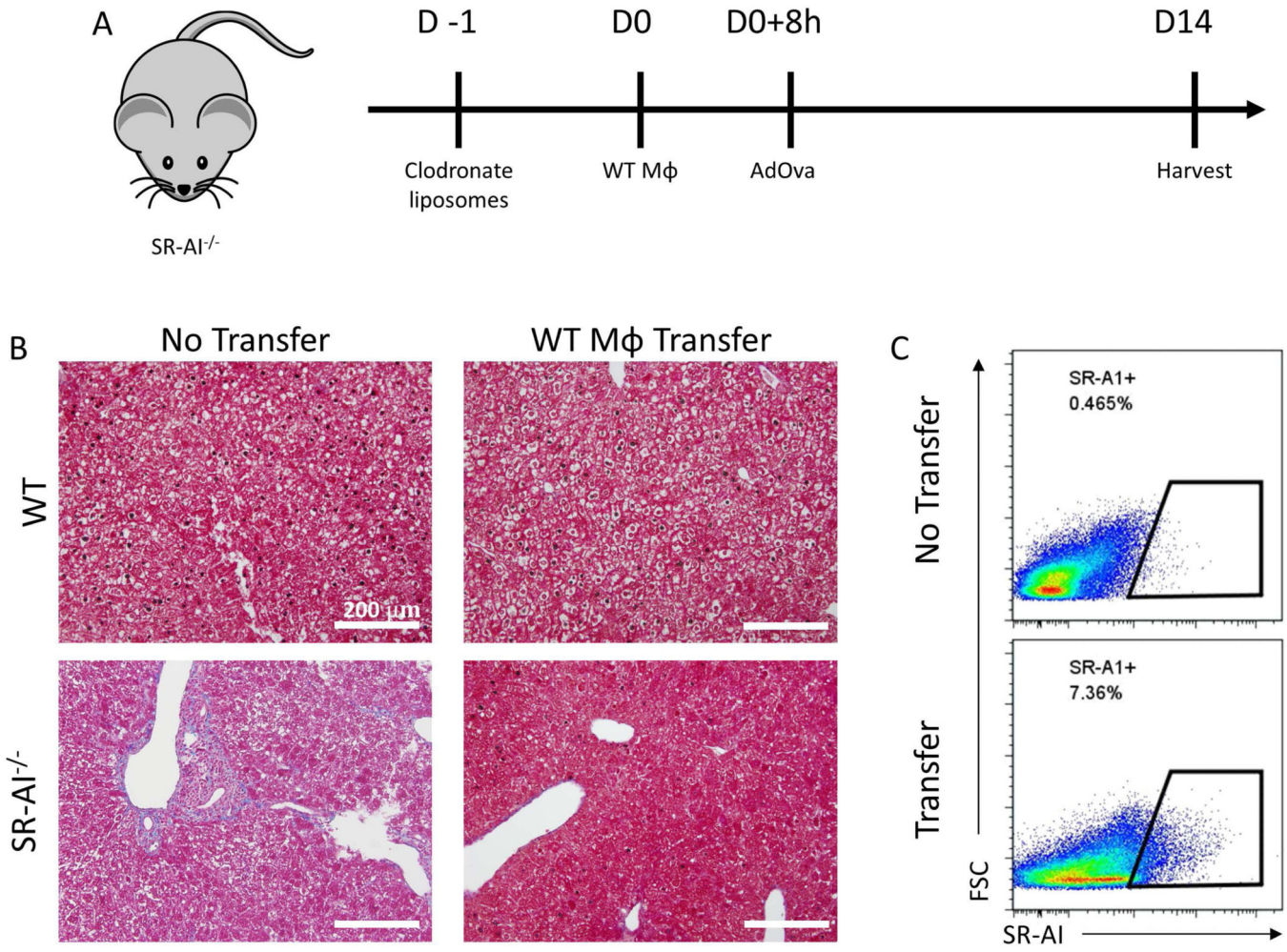

Figure 5. Transfer of SR-AI+ Mϕ protects against infection-induced tissue damage

(**A**) Experimental design for adoptive BMDM transfer and infection. (**B**) Trichrome staining for collagen in liver sections from WT and SR-AI$^{-/-}$ mice 14 days post infection (× 100 magnification and scale bars = 200 µm). Images representative of 3 mice. (**C**) Confirmation of successful transfer of SR-AI^{+} BMDMs into SR-AI$^{-/-}$ mice by flow cytometry.